CEMENTATION AND TECTONICS IN THE
INNERALPINE MOLASSE OF THE LOWER INN VALLEY

Hugo Ortner

With 12 figures and 3 tables

Abstract

Precipitation of large amounts of cement in and below Inneralpine Molasse in the Lower Inn Valley is tied to distinct tectonic events: (1) faulting during rapid subsidence created porosity in the basement of the basin. Important fluid flow, hydrocarbon migration and precipitation took place in these fault systems during the thermal climax of the basin. Compressive movements terminated subsidence in the Lower Miocene. (2) Younger shearing in the basin produced porosity again and led to precipitation of saddle calcites in the basin fill.
The age of cement generations can be determined with the technique of brittle microtectonics, as most cement filled veins are connected to faults. The kinematic development of an area provides a time frame for cementation.
It was tried, to discriminate between marine and meteoric sources of diagenetic fluids by comparing the trace element composition of calcite cements precipitated from the fluids with Oligocene marine and meteoric carbonates. The chemistry of fluids circulating in the basins subsurface changed from predominantly marine to meteoric through time, as observed also in other basins. The change took in pore water chemistry took place in short time, because all cements in the basin subsurface are found along faults of the same generation.

Zusammenfassung

Ausfällung von großen Mengen an Zement in den den Ablagerungen der inneralpinen Molasse im Unterinntal und in älteren Gesteinen darunter ist an tektonische Ereignisse gebunden: (1) Scherung während der Beckensubsidenz erzeugte Porosität in den das Becken unterlagernden Gesteinen. An den Störungen stiegen Kohlenwasserstoffe und diagenetische Lösungen auf, und es kam zur Ausfällung von großen Mengen an Kalzit während der maximalen Aufheizung des Beckens im Oligozän. (2) Jüngere, miozäne tektonische Bewegungen führten zur Entwässerung des Beckeninhaltes und zur Ausfällung von Sattelkalzit an Störungen. Das Alter der Zemente wurde durch die Störungen, an die sie gebunden sind, bestimmt. Die kinematische Geschichte des westlichen Kalkalpen bietet den Zeitrahmen, in den die Zementation eingehängt werden kann.
Es wurde versucht, mit Hilfe der Spurenelementzusammensetzung von Kalziten die Herkunft der Lösungen zu bestimmen, aus denen die Kalzite ausgefällt wurden. Die Zusammensetzung der diagenetischen Lösungen im Beckenuntergrund veränderte sich mit der Zeit von marin zu meteorisch, wie es auch in anderen Becken beobachtet wurde. Die Umstellung beansprucht sehr geringe Zeit, da alle Zemente an dieselben tektonischen Strukturen gebunden sind.

1 Introduction

Fluid migration in orogens is usually triggered by deformational events. Brittle faulting in shallow parts of the crust opens porosity for fluid migration and precipitation from the fluid (e.g. Sibson, 1983). Fault zones are thought to be major fluid migration paths. The presence of overpressured fluids in thrust faults is a prerequisite for large distance thrusting of thin thrust units (Hubbert & Rubey, 1959). Usually stretched calcite or quarz fibers are precipitated from the fluid, which can be used for microtectonic investigations (e.g. Petit, 1987). This opens the possibility to find the age of cementation indirectly, because the age of tectonic events is more easy to define than the age of cements.

Following Eocene continental collision of the Adriatic microplate and the European plate, a peripheral foreland basin formed north of the Alps. The northern part of the Eastern Alps was part of the foreland basin, and subsided together with the foreland basin (Ortner & Sachsenhofer, 1996; Ortner & Stingl, 2001). The Oligocene sedimentary succession is therefore similar to the western Molasse basin. However, on a local scale the distribution of facies was controlled by faulting in the basins subsurface.

Faults in the subsurface of the basin and in the basin fill locally show evidence for important paleo-fluidflow. Besides the development of stretched calcite crystals on slickenside surfaces, thick calcite veins occur, partly associated with breccias. Together with paleo-temperature data (Ortner & Sachsenhofer, 1996), an investigation of C- and O-isotope values of calcites from faults with known age allows to differentiate between cements precipitated from fluids in thermal equilibrium with the hostrock and hydrothermal fluids. A first estimate is made on the role of diagenetic fluids from deeper parts of the basin and meteoric fluids, that both contributed to precipitation of cements in the observed outcrops. The diagenetic history of the basin is reconstructed.

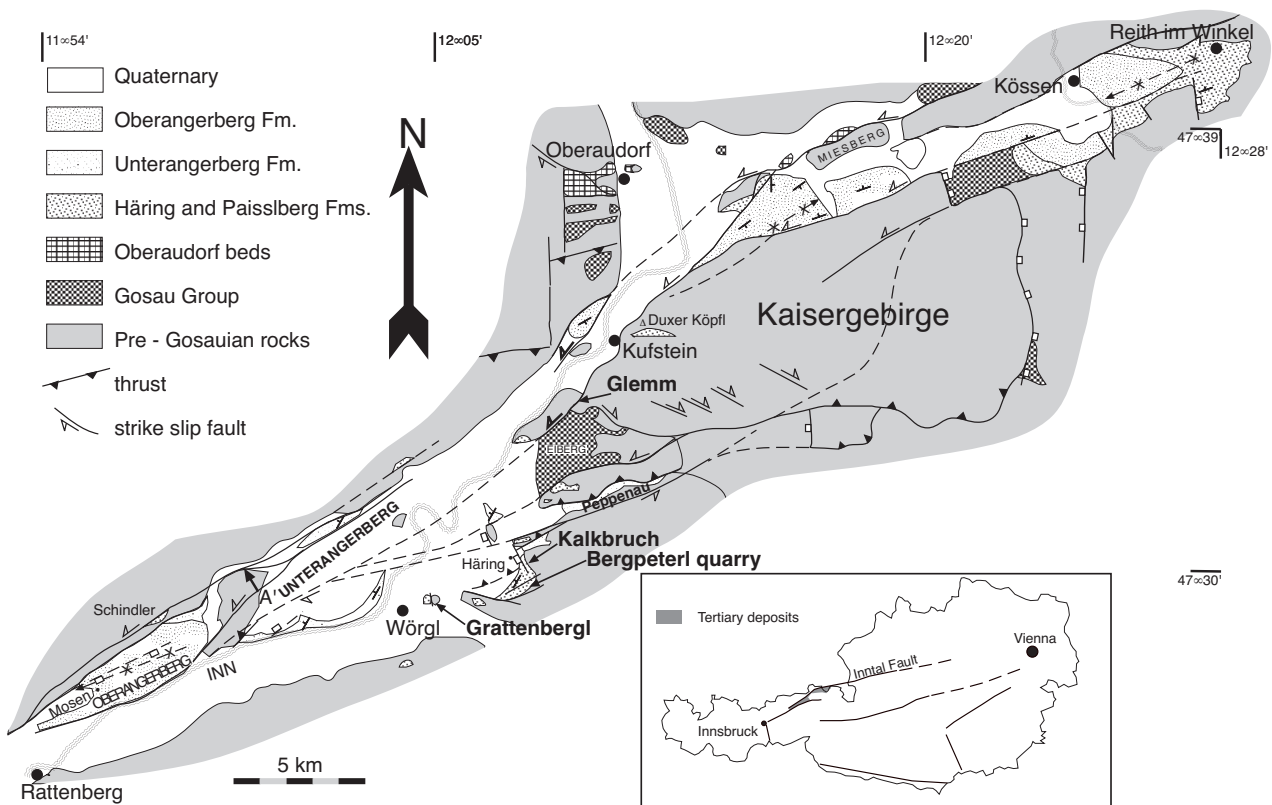Oligocene deposits on top of the already deformed nappes of the Northern Calcareous Alps are preserved

Fig. 1: Geologic sketch of the Inntal Fault and the Tertiary basin. Inset shows the orientation of major Tartiary faults in the Alps and the position of the Inneralpine Molasse deposits.
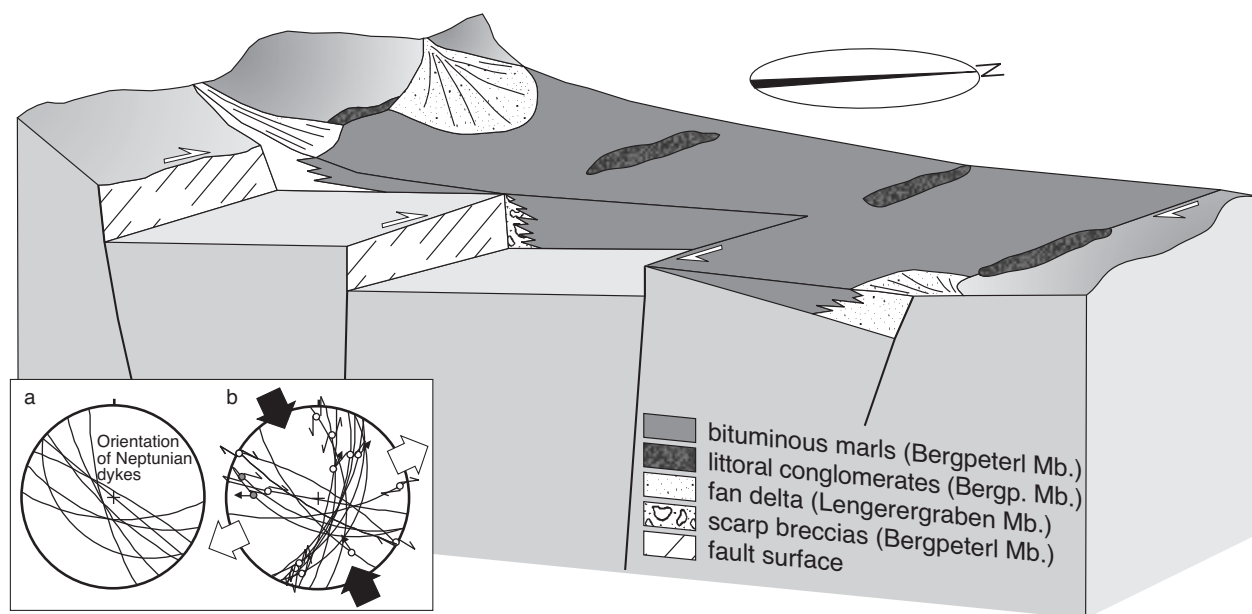
Fig. 2: Block diagram of the Inntal area in the Early Rupelian (D1). WNW–trending dextral faults dissected the area and formed half-graben shaped small restricted basins. Inset: a) Orientation of neptunian dykes filled by flowstones and debris from Werlberg Mb., b) brittle fault plane data set compatible with a) indicating NNW-SSE directed compression. Faults with grey symbols are sealed by Oligocene sediments.

in a syncline-anticline system, which is cut by the Inntal fault (Fig.1). Oligocene deposits overly both the Bajuvaric and the Tirolic nappes, which are separated by the Inntal fault in the investigated area. Southeast of Salzburg, lower Oligocene deposits were drilled below the Tirolic nappe, proving post-(Early)Oligocene thrusting of the Tirolic onto the Bajuvaric nappe (Vordersee 1 well; Tollmann, 1986, p. 169). The sinistral Inntal fault is a major fault in the Eastern Alps, mainly active during post-collisional (post-Eocene) orogen-parallel extension in the Eastern Alps, delimiting eastward moving units to the south against more stable units in the north of the fault (Ratschbacher et al., 1991, Ortner & Stingl, 2001).

2 Tectonic and sedimentary history of the area

As previously mentioned, the distribution of sedimentary facies in the Unterinntal area was controlled by faulting in the basins subsurface. Oligocene deformational events are illustrated in two block diagrams, that summarize the tectonic and sedimentary history.

D1 (Fig. 2): In Early Oligocene times, topopraphy was created by block faulting along WNW-trending

dextral faults. Bituminous marls (Bergpeterl Mb. of Häring Fm.) filled the half grabens, which interfinger with scarp breccias along the faults in internal parts of the basin and with breccias, conglomerates and sandstones (Lengerergraben Mb. of Häring Fm.) deposited in fan deltas at the southern and northern basin margin (Stingl & Krois, 1991; Stingl, 1990; Ortner & Stingl, 2001). Brittle faults associated with this deformational event (see example in inset c of Fig. 2, inset a and b) are occasionally karstified and filled by Oligocene carbonates, proving also a pre-Oligocene age of faulting. Brittle fault data sets show conjugated WNW-striking dextral and N-striking sinistral faults and were formed during NW-SE compression.

D2 (Fig. 3): Pelagic calcareous marls (Paisslberg Fm.) overlie the bituminous marls. In their lower part, they interfinger with breccias (Werlberg Mb. of Paisslberg Fm.) shed from intrabasinal highs and from the basin margins, where shallow marine conditions prevailed. Toward the top, the amount of silicicalastics increases, and the calcareous marls grade into turbiditic sand – marl couplets (Unterangerberg Fm.). The distribution of shallow water carbonates and calcareous marls was controlled by faulting along ENE-striking faults, until the strong subsi-
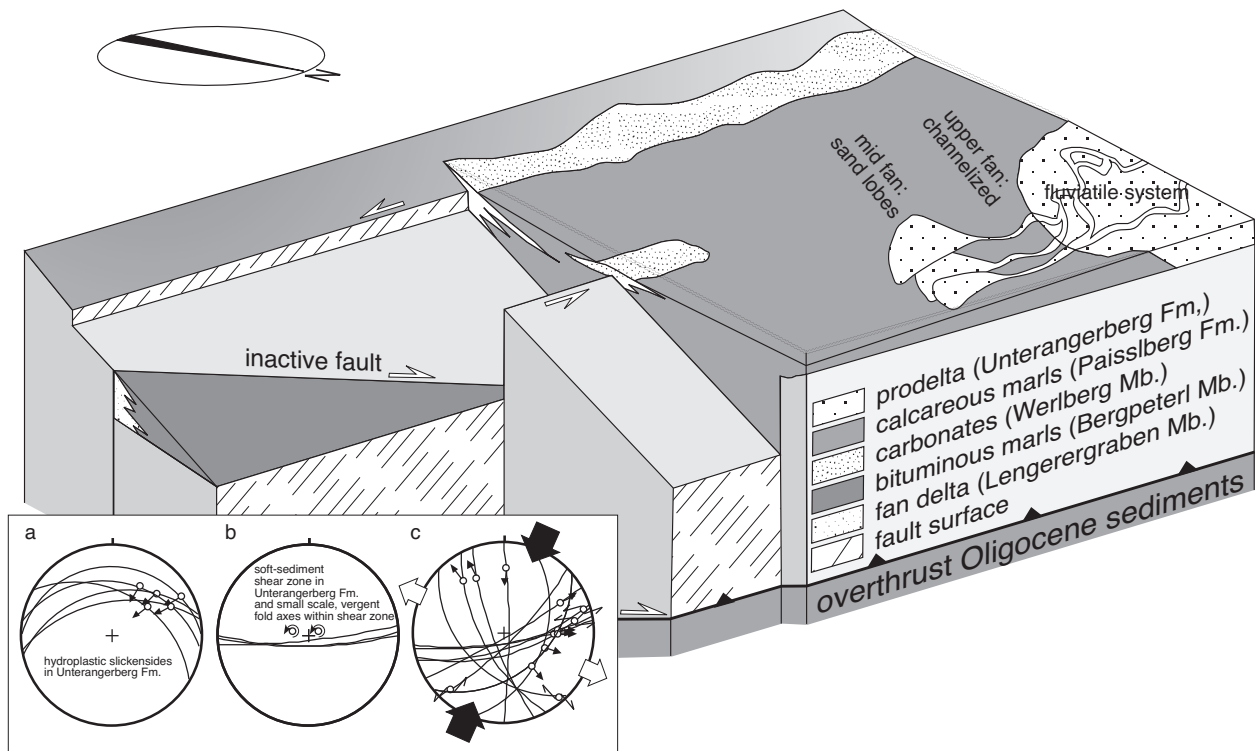
Fig. 3: Block diagram of the Inntal area during deposition of calcareous marls (Paisslberg Fm.) and younger turbidites (Unterangerberg Fm.) in the Late Rupelian (D2). Oligocene carbonates (Werlberg Mb.) rim the southern margin of the basin and isolated horsts inside the basin. Fault blocks between active sinistral faults show half graben geometry. Sinistral faulting is contemporaneous with oblique NE-directed thrusting. From the west, a fluviatile system approaches, with the Unterangerberg Fm. in a prodelta position. Inset: a) Top SW reverse faults with hydroplastic slickensides indicate activity before final lithification, b) shear planes in pseudoductile shear zone (great circles) and small scale fold axes with vergence of folds indicating a sinistral shear sense, c) brittle fault plane data set compatible with b) indicating NNE-SSW compression.

dence drowned the shallow water domains. Soft sediment deformation in the Unterangerberg Fm. shows, that sinistral faulting along ENE-striking faults, thrusting and sedimentation was contemporaneous (Ortner, 1996, 1999; Ortner & Stingl, 2001). Tension gashes formed during soft sediment faulting are mineralized with saddle calcites.

The turbiditic succession is overlain by fluviatile conglomerates (Oberangerberg Fm.) of Chattian age (Zöbelein, 1955; Ortner & Stingl, 2001). The preserved thickness of these conglomerates is about 1000 m (Ortner, 1996). A simulation of the thermal history of the basin demands a thickness of about 1500m for the fluviatile deposits (Ortner & Sachsenhofer, 1996).

Deformation events younger than Oligocene can only be dated relatively. The correlation to major tec-

tonic events in the Eastern Alps provides a time frame. The Oligocene deposits are overprinted by two tectonic events. Initially they are folded on a kilometric scale with WSW-trending axes (Fig. 4a, b). Brittle fault sets attributed to this deformational event show dextral, WNW-striking and sinistral, N-striking fault planes (D3; Fig. 4c). Brittle faulting obviously postdated folding, because the fault sets are not tilted. In Oligocene rocks, these faults are partly mineralized with thick veins of saddle calcite.

D4: Renewed sinistral shearing along the Inntal fault overprints the Oligocene sediments and the D3 fault planes. Sinistral faults are oriented NE-SW to ENE-WSW, dextral faults N-S, indicating NE-SW shortening (Fig. 4d). This event develops from transpression to transtension (Ortner, 1996; Peresson & Decker, 1997). Faults from transpressive datasets within the calcareous marls are mineralized with
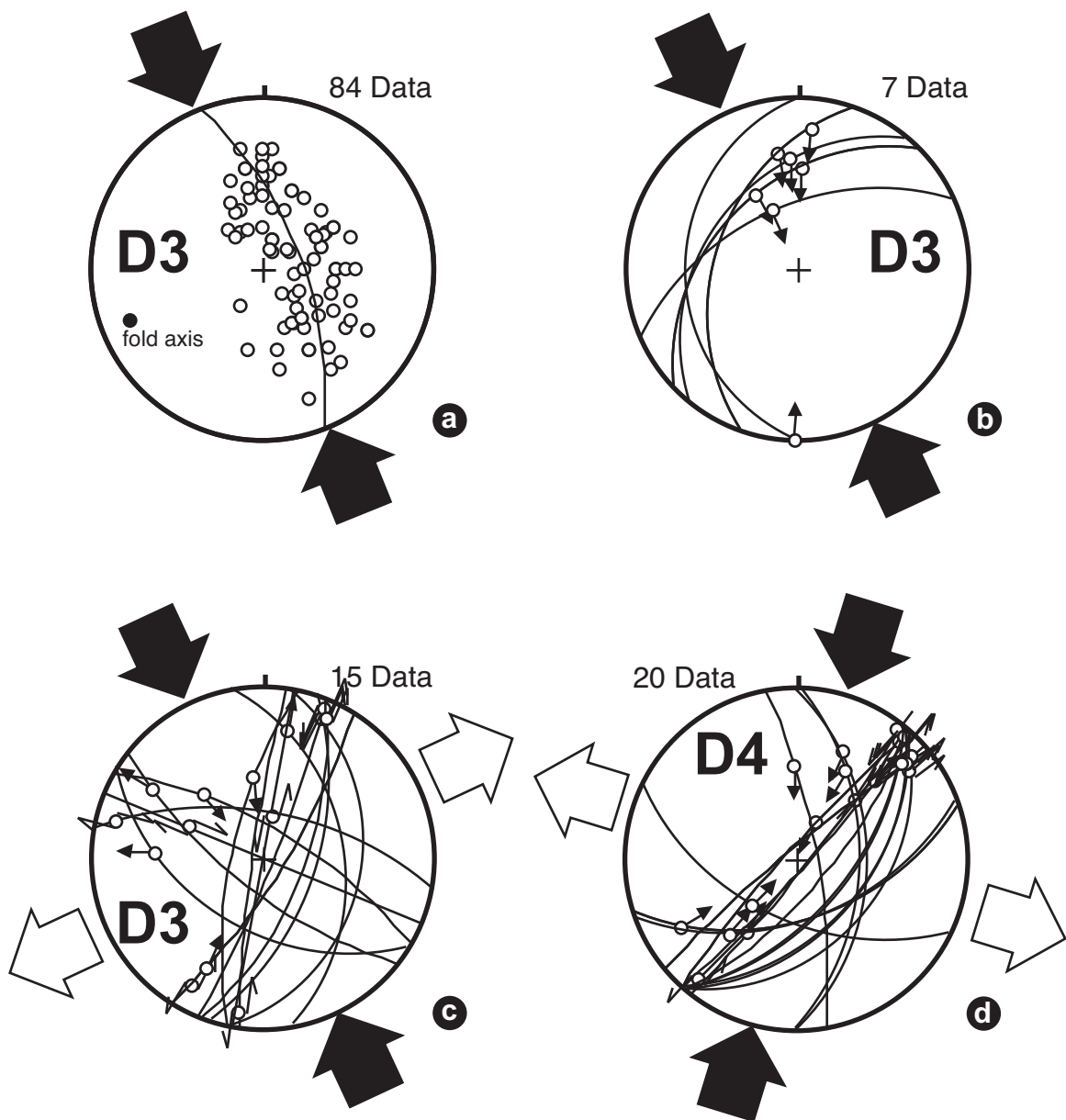
Fig. 4: Examples of D3 and D4 brittle fault sets from the Unterinntal area. a) poles of bedding planes of Chattian fluviatile conglomerates of the Oberangerberg (Fig. 1) show post-Chattian NNW-SSE contraction (D3). b) slickensides in Oligocene calcareous marls (Bergpeterl quarry) formed by flexural slip during folding indicate NNW-SSE contraction (D3). c) Fault planes related NNW-SSE contraction (D3) in Oligocene calcareous marls of the Bergpeterl quarry. d) Fault planes related to NNE-SSW contraction (D4) in Oligocene calcareous marls of the Bergpeterl quarry. Faults depicted in c) and d) are not affected by tilting and postdate post Chattian folding of a).

saddle calcites, whereas faults from transtensive and transpressive data sets in Triassic rocks below the Oligocene are associated with important cementation. Sinistral activity of the Inntal fault was interpreted to be caused by orogen parallel extension in the central part of the Alps in the Middle Miocene (Ratschbacher et al., 1991).

3 Cements of Oligocene and older rocks

The cement stratigraphy in Tertiary sediments and in the Triassic rocks below was investigated in two large quarries at the southern margin of the Tertiary basin near Häring. In the quarry "Bergpeterlbruch" Oligocene calcareous marls are mined. In the quarry

"Kalkbruch Perlmooser" Wetterstein limestone (Ladinian carbonate platform) is exploited. The Grattenbergl, the third sampling locality, is a horst of Wetterstein limestone inside the basin near Wörgl (Fig. 1).

Carbonate cements in the Tertiary sediments and in the Wetterstein limestone below were characterized petrographically in thin section, and carbon and oxygen isotopic composition and concentrations of iron, manganese, magnesium, strontium, barium and zinc were determined. Cathodoluminescence was not useful, because all Tertiary cements had a uniform dull orange luminescence. Cross-cutting relationships between cements in veins were used to establish the relative age of individual cement generations. Stretched calcite fibers at vein walls were used to relate cements in a vein to the tectonic event responsible for opening the vein. Cross-cutting relationships of veins with faults were used to define relative ages to fault sets.

3.1 Petrographic description and isotopic composition of cements

Three generations of cements can be distinguished in the Wetterstein limestone below the Tertiary sediments:
1) pre-Tertiary cements, mainly radial-fibrous calcite and blocky spar
2) flowstones and caliche crusts that formed prior to the Oligocene sedimentation
3) Oligocene blocky spar

In detail, the cement stratigraphy varies from outcrop to outcrop. Oligocene cements are particularly variable.

3.1.1 pre–Tertiary cements

Primary voids in the Wetterstein limestone are filled by isopachous fringes of fibrous calcite (Fig. 5a). Parts of the Wetterstein limestone are brecciated and cemented by a first generation of radiaxial-fibrous calcite and then a generation of sparry calcite (Fig. 5b). All these cements show intrinsic luminescense. Another type of calcite found in the Kalkbruch area are large clear columnar crystals of calcite up to 3cm high, that fill tectonically opened voids ("Kanonenspat", compare Kuhlemann, 1995, Weber 1997).

Carbon and oxygen stable isotope values of the Wetterstein limestone (bulk-samples) and most of its cements range between +2 to +4‰ and −2 to −5‰, respectively. Only the blocky spars have more negative oxygen values between −6 to −8‰, and the columnar calcites range from −11 to −15‰ (Fig. 6a). All these values are within the range of previously published data for matrix calcite and cements of the Wetterstein limestone (e.g. Zeeh et al., 1995; Weber, 1997).

3.1.2 Speleothems and spring tufas formed prior to the Oligocene sedimentation

Before the onset of sedimentation in the central part of the basin, a period of subaerial exposure is recorded by the development of karst features in the Triassic Wetterstein limestone. Solution widened faults and joints are filled by a rythmical alternation of spring tufas and flowstones. These cements occur both in the localities Grattenbergl and Kalkbruch.

The wall rock and the flowstones are often brecciated and resedimented in the next tufa crust (pedogenic breccias). In one well-preserved sample a lamination in the flowstones produced by organic matter sedimented on the growing calcite crystals is preserved (Fig. 5c), but generally the flowstones are intensely recrystallized and the laminations are poorly preserved (Fig. 5e). Under ultraviolet light, the flowstones show fluorescent growth laminae very similar to present-day speleothems. The tufa crusts show variable textures, mostly alveolar fabrics (Fig. 5e), rhizolithes (Fig. 5d), mottled micritic fabric, and abundant pellets (Fig. 5e). Because of fault movements and/or formation of pedogenic breccias during growth of the calcretes, these are laterally discontinuous, and it is not possible to establish a systematic stratigraphy of alternating flowstones and certain types of crusts within the study area. The youngest part of these fissure fillings are algal crusts, that grew along the margins of the fissure. The crusts resemble small stromatolites (Fig. 5f) which grew from the dyke fill to the dyke walls after renewed opening of the joint. $\delta^{18}O$ of carbonate crusts and speleothems ranges from −3 to −7‰, and most samples plot on the meteoric calcite line
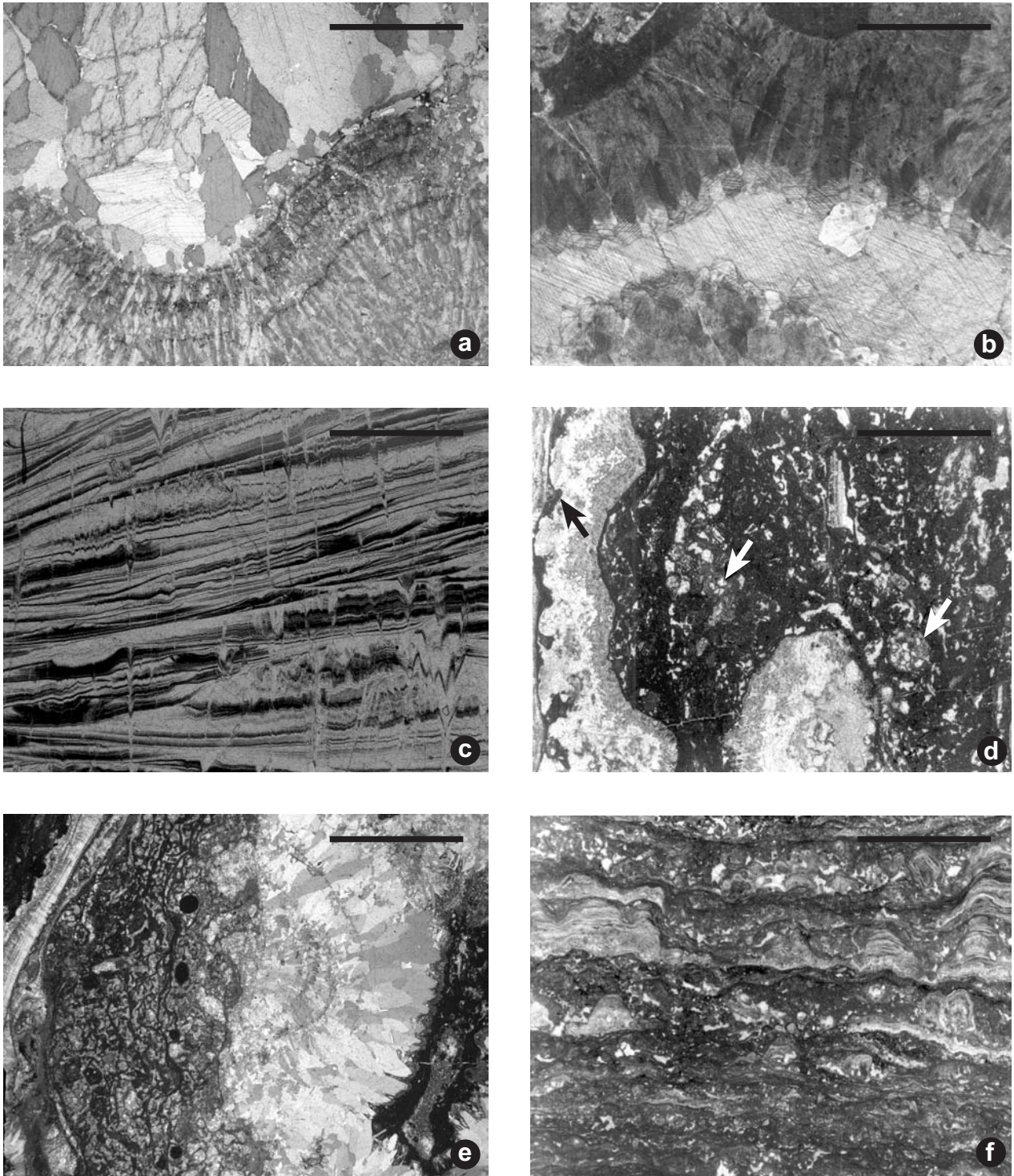
Fig. 5: Pre-Oligocene cements of the Wetterstein limestone: a) First generation of cements in the Wetterstein limestone (Grattenbergl locality, sample G1): Fibrous calcite lining cavity walls (1), overgrown by Oligocene blocky calcite (2). b) Second generation of cements in the Wetterstein limestone (Grattenbergl locality, sample G8): radiaxial fibrous cement (RFC) filling a void (1) followed by blocky spar (2). Initally, the crystals of the RFC continued to grow with the same optical orientation, but with straight twin lamellae. Spring tufas and flowstones predating Oligocene sedimentation: c) Well preserved flowstone from a pre-Oligocene karst void (sample GB3). Dust layers in the crystal record periodical growth of the flowstone. d) Alveolar structure with rhizolithes (white arrows) in a tectonically opened joint (sample G4/2). On the left hand side a layer of flowstone growing over dripstone cements (black arrow). e) Fill of a karstic dyke with (from top left to bottom right; sample G4/2): "Terrestrial stromatolite" (see also Fig. 5f), flowstone, alveolar structure with pellets, recrystallized flowstone (the dust layers are only left as ghost structures, compare Fig. 5c) f) "Terrestrial stromatolithes" in a tectonically opened joint (sample G4/2). These structures occur in association with tufa crusts. Bar is 5mm in all photomicrographs.
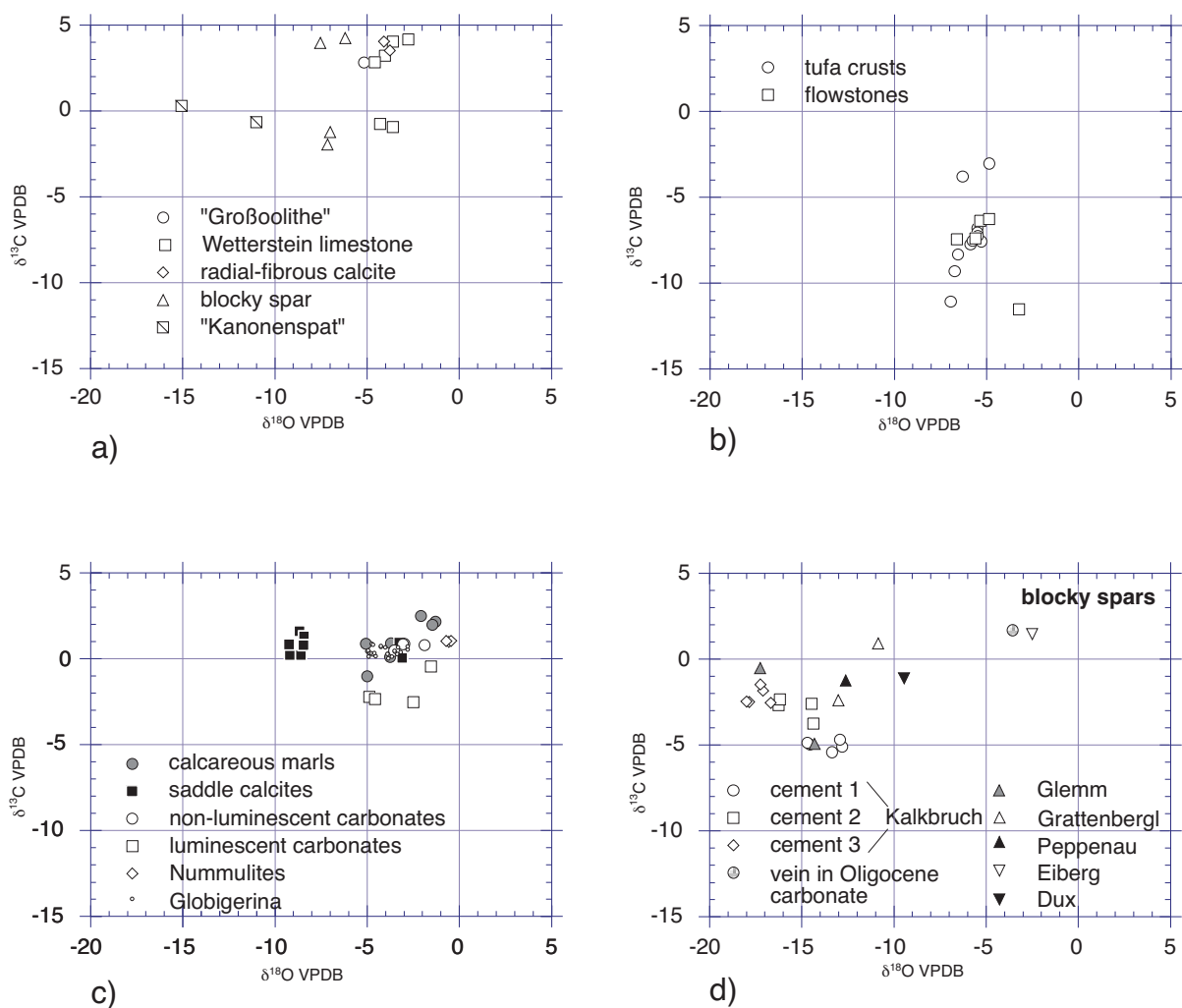
Fig. 6: Isotopic values for the measured calcite cements a) Wetterstein limestone and pre-Tertiary cements. b) Tertiary calcretes and flowstones. c) Oligocene carbonates, calcarous marls and saddle calcite within the calcareous marls. Isotope values for Globigerina taken from Scherbacher (2000). d) Oligocene blocky spars from the basins subsurface.

(Lohmann, 1988), δ13C values vary between –12 to –3‰ (Fig. 6b).

3.1.3 Karst voids and solution widened faults filled by Oligocene sediments

Other solution-widened faults at the Grattenbergl outcrop are filled by debris from fossiliferous Lower Oligocene carbonates, resembling the Werlberg Mb. of the Paisslberg Fm. (see above). The walls of these NW-striking faults display slickensides, which indicate dextral movements before opening and filling (depicted in Fig. 2, inset b, faults with grey symbols); the carbonate debris seals the fault.

The innermost fill of a solution-widened fault at the Grattenbergl location with alternating speleothems and tufas (see above) is a packstone containing foraminifera of Early Oligocene age (det. W. Resch). Karst voids in the Wetterstein limestone of the Grattenbergl are filled by laminated silty carbonate that occasionally contains small foraminifera. Flowstones as described above are reworked into these karst void fills. The sediment in the cavities can be compared to the calcareous marls of the Paisslberg Fm.

Locally, karst voids filled by calcareous marls are found in autochthonous carbonates of the Werlberg Mb. (at the type locality of the Werlberg Mb.; Ortner
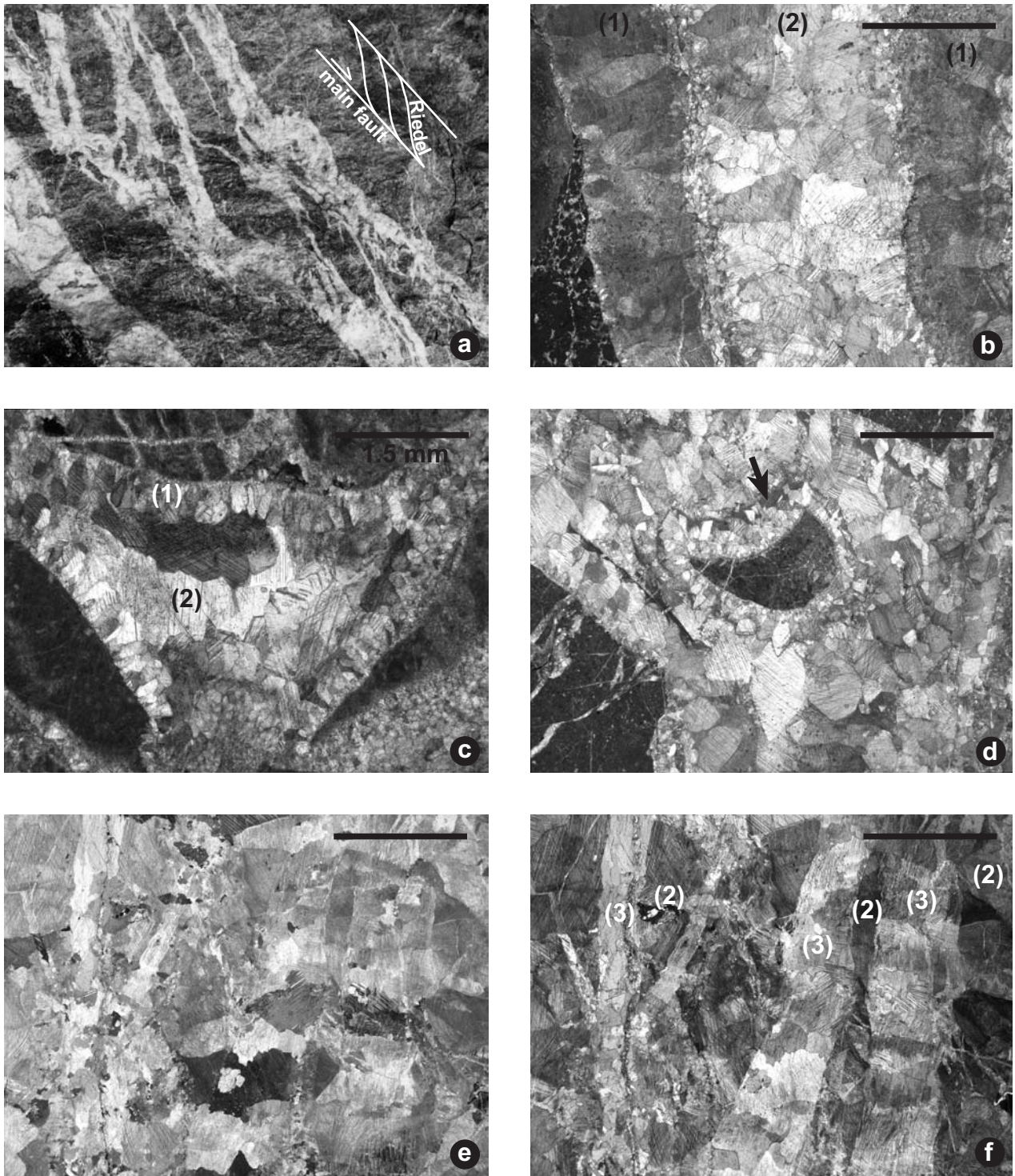
Fig. 7: Blocky spars of Oligo-Miocene burial diagenesis: a) Field example of normal fault in the Kalkbruch cemented with cement 1 and 2. The veins are up 75cm thick. The rock fragments within the vein show Riedel geometry. b) Cements 1 and 2 (sample KB2). Cement 1 shows growth lamination, cement 2 is a clear blocky spar. c) Cement 1 and 2 in a tectonic breccia (sample KB4). Cement 1 lines cavity walls, cement 2 is a blocky spar. d) Cement 2 in a tectonic breccia (sample KB4). Here cement 2 grows directly on Wetterstein limesto-ne. An older generation of cement 2 is separated from a younger one by a layer of crystal silt (black arrow). e) Cement 3 in veins in ce - ment 2 (sample KB1). f) Same view under crossed Nicols. Cement 3 grew in optical continuity with cement 2 and is therefore not easi-ly seen in Fig. 7e. Bar is 5mm, except Fig. 7c.

tufas, Speleothems

Cement 1,2,4

Kalkbruch

- ● Sigma 1
- ■ Sigma 2
- ▲ Sigma 3

oblique dextral normal faults of D2, comparable to the cemented faults to the left

Eiberg

Fig. 8: Orientation of the cemented faults and joint in the Kalkbruch locality: N-S trending joints and faults are filled by Oligocene blocky spar, NW-SE trending joints are filled by calcretes and tufas.

& Stingl, 2001, this volume). Therefore, repeated subaerial exposure and intermittent marine flooding is recorded by the different fills of the karst voids and solution widened faults.
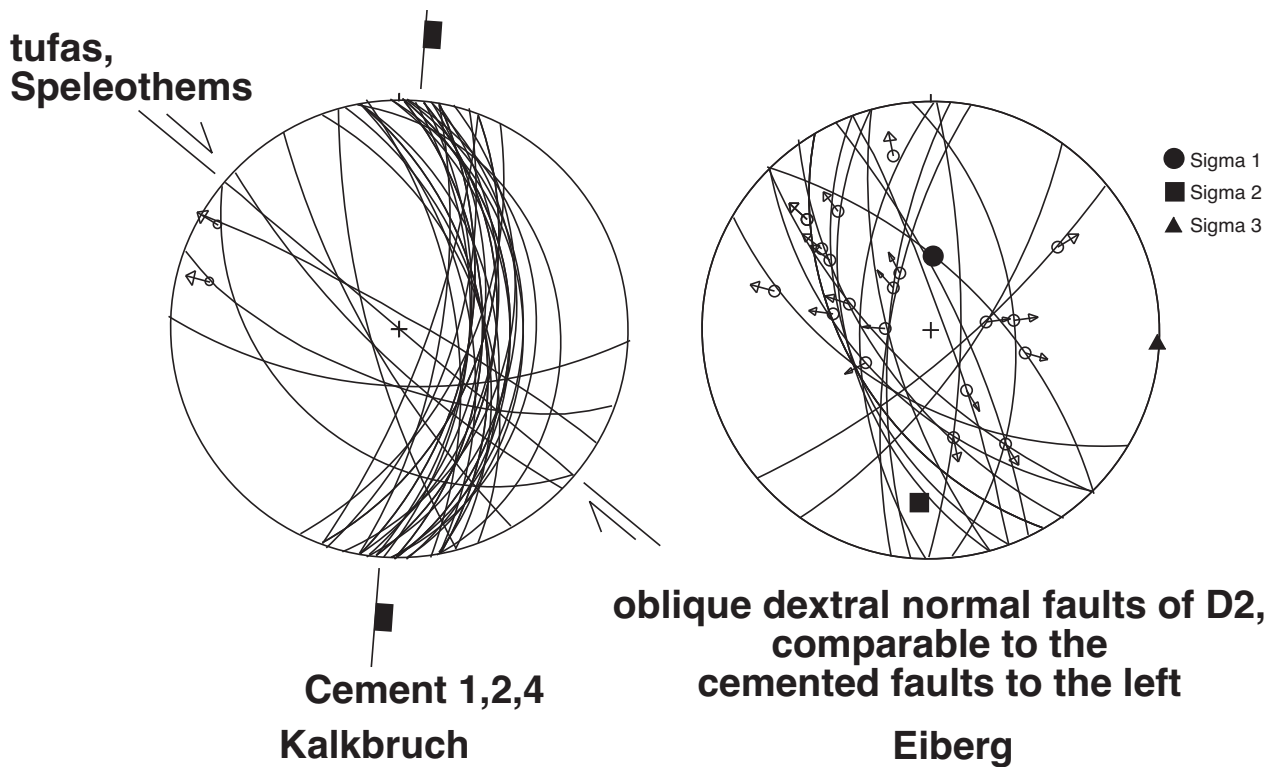
3.1.4 Blocky spars of the Kalkbruch outcrop

Younger cement filled faults, that are predominantly oriented N-S, cut the NW trending faults that contain tufas and speleothems. The N-S trending faults form so-called "fuzzy normal faults" (Sibson 1994), i.e., a network of cement-filled faults and fractures.

Some of these cement-filled faults are up to 75cm thick. The fault network in some of the thicker shear zones has a geometry of a master fault with associated Riedel planes and indicates normal faulting (Fig. 7a).

N-S-striking cemented normal faults (Fig. 8) are both compatible with Oligocene (D2) and Middle Miocene (D4) sinistral shearing. Some of the cement-filled veins are cut by NE-trending sinistral oblique reverse faults. Faults with a similar geometry are also found in the calcareous marls of the Paisslberg Fm. and formed during Middle Miocene transpressive sinistral shearing (Ortner & Stingl, 2001). Therefore, the age of the normal faults is interpreted to be Oligocene (D2).

Three generations of calcite can be distinguished macroscopically and/or in thin section in the Kalkbruch outcrop. The first generation, cement 1, is stained brown by bituminous material. In thin section, cement 1 is commonly laminated (Fig. 7b) and consists of prismatic spar growing on cavity walls (Fig. 7c). Cement 2 is a coarse, white spar, that has skalenohedral crystals if growing into voids. In thin section, it is a drusy calcite spar that locally forms fringe cements where brecciation had occured after precipitation of cement 1 (Fig. 7d). A third generation of blocky spar is present in some samples, where cement 2 is deformed by a crack-seal mechanism. In the cracks, the third generation of cement is precipitated in optical continuity with cement 2 (Fig. 7e, f). It is characterized by its relatively high barium content (up to 600 ppm). This cement is also present in

tension gashes in Oligocene carbonates in the Häring area (Fig. 9a). The orientation of these gashes (Fig. 9b) is compatible with NNE-SSW compression in the Oligocene (D2; see Fig. 3, inset c) and Miocene sinistral shearing (D4; see Fig. 4d). The crystals in the gashes, however, were not stretched during synkinematic growth, but they are blocky spars that filled a preexisting fissure. Calcite growth was interupted by tectonic movements, represented by a layer of crystal silt between two layers of blocky spar. Fragments of the wall rock are present along these zones. This indicates multiple fracturing and precipitation in these veins.

The carbon and oxygen isotope data show a trend for the Oligocene cements of the Häring area (Fig. 6d). The oxygen isotope ratio decreases from –13‰ (cement) to –15‰ (cement 2) to –18‰ (cement 3), while the carbon istope ratio increases from –5‰ (cement 1) to –3‰ (cement 2) to –2‰ (cement3). The trend goes to more positive carbon isotope ratios and more negative oxygen isotope ratios through time.

3.1.5 Blocky spars and skalenohedral calcites of other outcrops

The cement stratigraphy established for the Kalkbruch outcrop is not found in other localities. If porosity is present, either old or newly formed by faulting, clear skalenohedral calcite crystals grew. Voids in cataclasites in pre-Oligocene rocks along N–S trending faults in the Glemmschlucht near Kufstein (Fig. 1) are filled with up 10 cm long clear skalenohedral calcites. Porosity was formed by faulting along approximately N–S oriented dextral normal faulting associated to Oligocene sinistral shearing (D2); therefore the calcite directly overgrows older rocks. Two oxygen isotope values of these calcites are in the range of cements 1 to 3 in the Kalkbruch outcrop (Fig. 6d). Another sample of skalenohedral calcite crystals from a fault in Upper Cretaceous sandstones yielded oxygen and carbon isotope values of –2.5‰ and 1.5‰, respectively (Fig. 6d).

In the Grattenbergl outcrop early marine Triassic cements ("Großoolithe") and karst void fills with calcareous marls are overgrown by similar clear skalenohedral calcites. The remaining pore space is filled by bitumen. The oxygen isotopic composition

tension gashes filled with cement 3

Beach rock Häring

Oligocene carbonates Häring

Oligocene carbonates Bruckhäusl
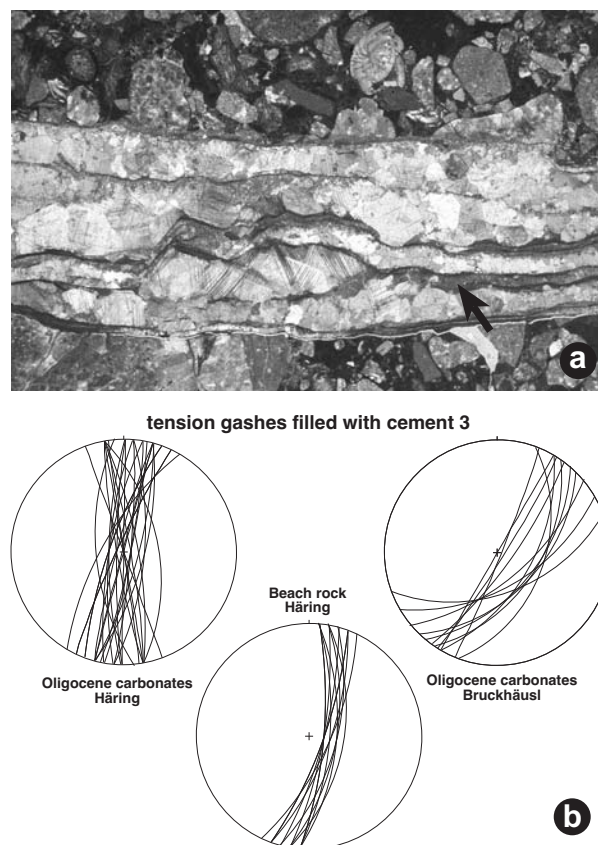
Fig. 9: a) Vein with cement 3 in Oligocene beach rock (sample OF10a). Crystals are not stretched, but crystallisation was interrupted by several phases of tectonic activity, represented by layers of crystal silt (black arrow). b) Orientation of veins with cement 3 in Tertiary carbonates.

of the calcites is comparable to cement 1, but the carbon isotope values vary between -3 and +1‰. The more negative values of $\delta^{13}C$ could be a effect of organic carbon from bituminous impregnation on and in the calcite crystals.

3.1.6 Cements within the basin fill

All brittle faults within the calcareous marls are associated with saddle calcite in up to 20cm thick veins (Fig. 10). Locally, barytocoelestin is present in the innermost part of those veins. Veins along sinistral NE-trending faults, that cut the Oligocene calcareous marls (Paisslberg Fm.) were sampled. The faults postdate folding of the Oligocene and therefore were formed during D4 in the Middle Miocene. The contacts of the calcite seams to the surrounding rocks show stretched calcite crystals and Riedel shear planes that continue into the surrounding

orientation of main fault   orientation of Riedel shear

stretched calcite crystal.

Fig. 10: Saddle calcites filling the central portion of a vein in the calcareous marls (Paisslberg Fm.). Stretched calcite crystals between secondary planes (Riedel planes) of the main fault plane are present along the margins of the vein. These calcite fibers are used in the field to determine the movement sense of the fault plane.

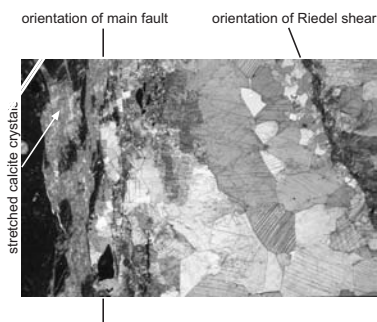sediment and the calcite vein (Fig. 10). Saddle calcite crystals are up to 1 cm large and show sweeping extinction under crossed polars. The stretched crystals at the contact to the country rock indicate synkinematic precipitation of the calcites. The oxygen and carbon isotope values vary slightly around –9‰ and +1‰, respectively.

Similar cements are present in NW-SE-trending tension gashes in the Unterangerberg Fm. at the Unterangerberg (Fig. 1). The tension gashes are parallel to the hinges of folds that formed in response to NE-SW contraction between larger ENE-striking sinistral faults active during the Early Oligocene (D2). In the Unterangerberg Fm., progressive contraction led to the formation of a set of structures, that allows to conclude that deformation in the Unterangerberg area started prior to lithification of the sediment (Ortner, 1999; Ortner & Stingl, 2001, this volume). Oxygen and carbon isotope values are in the range of –3‰ and +0.5‰, respectively (Fig. 6c).

3.1.7 Oligocene carbonates and cements within (Werlberg Mb. of Paisslberg Fm.)

Cathodoluminscence allows to distinguish two types of carbonates: Either the complete sample re-

mains dark, or the complete sample shows orange luminescence. The behaviour in cathodoluminescence is related to the isotope values from bulk analyses of the carbonates: The non-luminescent carbonates have carbon ratios around +1‰, and the luminescent carbonates yield carbon values around –2‰, the oxygen isotope value varies in both cases around –3‰, only a very slight shift to more negative values could be interpreted. Blocky spar in tension gashes in the carbonates shows isotopic values comparable to those of the surrounding (intrinsically luminescent) carbonate rock (Fig. 6c and d).

Tests of large foraminifera (nummulites) never show luminiscence. According to literature data, these foraminifera precipitate carbonate in isotopic equilibrium with sea water (e.g. Anderson & Arthur, 1983). Therefore, the data from individual nummulite tests are interpreted to represent a primary signal for the Oligocene sea water, with a carbon isotope value of +1‰ and a oxygen isotope value of –0.6‰. Compared to these data, all Oligocene carbonates show significally depleted $\delta^{18}O$ values, but only the luminescent carbonates show shifts toward more negative $\delta^{13}C$ values (Fig. 6c).

4 Trace element composition of carbonates and carbonate cements

The concentrations of strontium, magnesium, iron, manganese, barium und zinc in Triassic and Oligocene carbonates and cements were measured. Trace element distributions across veins can be used to decide whether the calcites were precipitated in an open or closed system (Erel & Katz, 1990). The data were also used to discriminate between cements precipitated from marine or meteoric solutions. Trace element data of the flowstones and tufas were taken as reference for carbonate cements precipitated from meteoric water, and data from Oligocene marine carbonates were taken as reference for carbonates precipitated from marine solutions.

4.1 Meteoric carbonates

Meteoric carbonates analyzed in this study are generally low in rare elements. The well preserved flowstones from the Grattenbergl are low in stron-
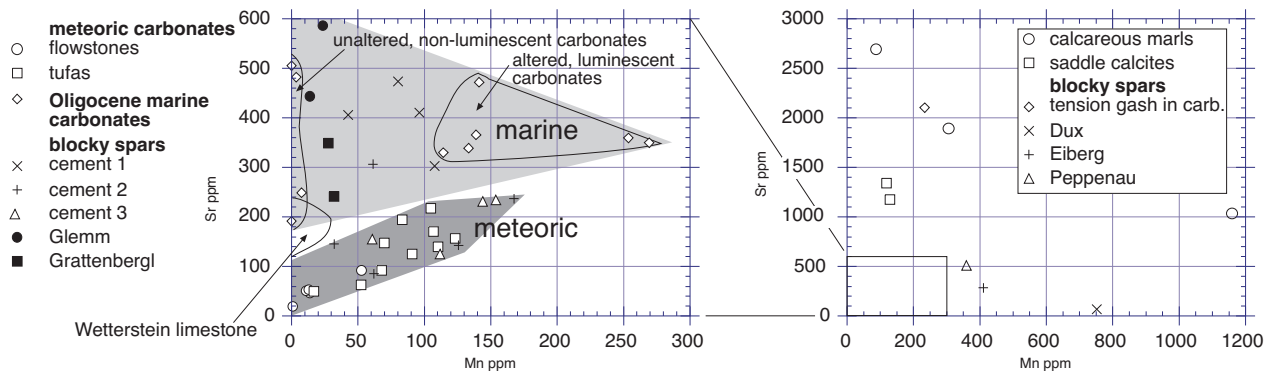
Fig. 11: Concentrations of Sr and Mn in samples from Oligocene rocks and cements. For discussion see text.

tium, iron, manganese, barium und zinc, only magnesium is more abundant. The recrystallized flowstones (Fig. 5e) display slightly higher contents of all trace elements.

4.2 Marine carbonates

In a crossplot Sr versus Mn (Fig. 11), a marine field with Sr values larger than 150ppm is defined by the values of the Wetterstein limestone and the Tertiary limestones, and a meteoric field is defined by the values of the flowstones and calcretes. Altered, luminescent and unaltered, non-luminescent Oligocene marine carbonates were sampled, and the altered samples show higher Mn- and Fe-concentrations, whereas Sr- and Mg-concentrations remain constant. Increasing Mn- and Fe-concentrations are obviously a result of diagenesis. Meteoric diagnesis would lead to a drop in Sr, as meteoric waters have relatively low concentrations of trace elements. Therefore, alteration of the marine carbonates is regarded to be due to marine diageneses, with minor meteoric influence shown by a shift toward more negative d13C values. The very high Sr-concentration of calcites in tension gashes in the Oligocene carbonates suggests, that dewatering of the calcareous marls, which are rich in trace elements and and especially in Sr, provided the fluid for marine diagenesis.

4.3 Calcareous Marls and associated carbonate cements

The calcareous marls are extremely rich in trace elements. Their Fe and Mg contents are about 10 times higher than those of the marine carbonates.

One source for these elements is montmorillonite, which is a important constituent of the calcareous marls (Czurda & Bertha, 1984). Leaching of these minerals during sample dissolution could have supplied the high amounts of these elements. Biogenic carbonate precipitated as aragonite is a possible source for Sr, because aragonite can be extremely rich in Sr (Kinsman, 1969). Cements precipitated in the calcareous marls ("saddle calcites") have similar high contents of trace elements, but much much less Mg. Dewatering of the calcareous marls possibly provided the fluid.

4.4 Blocky spars

Cement 1 in the cement succession is interpreted as a marine precipitate, as is plots with the Tertiary carbonates in the Sr/Mn plot (Fig. 11). Cement 3 plots together with the flowstones and is interpreted as a meteoric cement. Most cement 2 samples plot close to the meteoric carbonate field. The blocky spars from the Grattenbergl and Glemm localities are relatively rich in Sr and poor in Mn and plot with marine carbonates, the other samples of blocky spars are rich in trace elements and plot with the calcareous marls. Higher Sr-concentrations associated with higher Mn-concentrations in cements 2 and 3 suggest, that that some marine connate water was added to the fluid dominated by a meteoric source. Fluid mixing was inhomogeneous, so that some of the cements show a meteoric, others a marine trace element signature.

All Oligocene blocky spars analyzed in this study show trace element compositions typical for the fluid, from which they were precipitated, and differ-
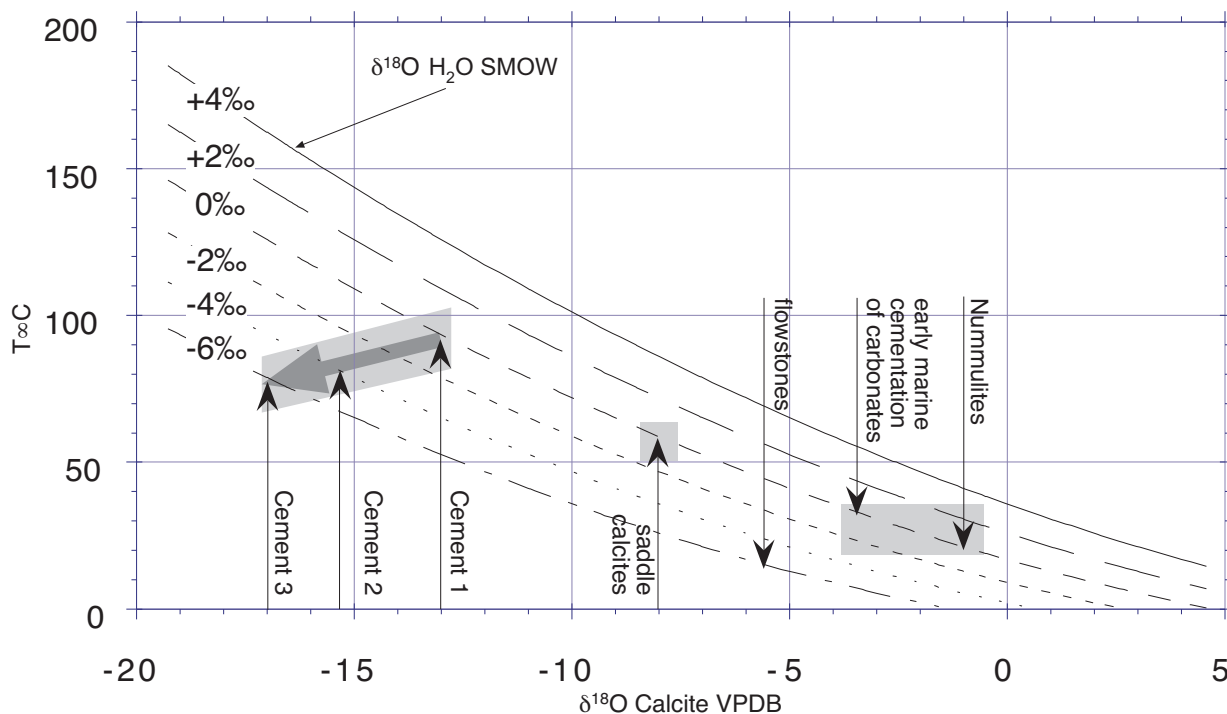
Fig. 12: History of cementation in the Inn Valley basin. The earliest cements precipitated during early marine cementation from marine waters. The major cementation event occured during Oligocene basin subsidence, when cements 1, 2 and 3 were precipitated at temperatures around 90°C. The shift in δ18O is interpreted as an effect of change in pore water composition from marine (connate) waters to meteoric waters. Precipitation of saddle calcites during Miocene faulting occured at slightly elevated temperatures around 60°C (for dicussion, see text).

ent from the trace element composition of the wall rock. Therefore, all cements were precipitated in an open system with large amounts of fluid passing through the system (compare Erel & Katz, 1990).

5 Discussion and Conclusions

Diagenesis of the Tertiary sediments and the rocks in the subsurface during basin evolution can be linked to depositional and tectonic processes and can be subdivided into several stages:
1) Karstification of pre-Oligocene rocks and depositi- on of flowstones and tufas in solution-widened faults and karst cavities during a period of erosion before the onset of Oligocene sedimentation.
2) Filling of karst voids and preexisting faults by Oli- gocene deposits (equivalents of bituminous marls, carbonates and calcareous marls) during sedimen- tation in the basin.
3) Burial diagenesis in the basement of the basin and in the basin-fill during the Oligocene. The basin was filled with about 2000m of sediment, and ac- cording to thermal history modelling, maximum

temperatures of about 90°C were reached by the end of the Oligocene (Ortner & Sachsenhofer 1996), followed by slow cooling to about 60° in the Middle Miocene.

If the chemistry of of a fluid is known, paleotem- peratures of the fluid can be calculated from the oxygen isotope value of the calcite precipitated from the fluid. Several expressions were suggested in lit- erature, and the expression by Craig (1965) is widely used (e.g. Anderson & Arthur, 1983; Tucker & Wright, 1990; Fig. 12). The chemistry of the diagenetic fluids cannot be exactly reconstructed, because the trace element analysis shows, that fluid mixing between marine and meteoric fluids was important for most cements, and the ratio of the two fluids is unknown.

The fluid evolution at the locality Kalkbruch is known best. Sucessive precipitation of cements 1, 2 and 3 took place under increasing admixture of a meteoric fluid to a marine fluid, as reconstructed by trace element analysis. The relatively negative δ13C values of cement 1 could be a result of the impreg- nation or incorporation of cement 1 by bitumen. If a

small amount of the organic material is solved during sample preparation, the d13C values will show a strong shift toward more negative values, because organic material has very negative carbon isotope values. Cement 1 was precipitated during hydrocarbon migration from deeper parts of the basin. Source rocks in the investigated area are the bituminous marls, however, these did not reach the oil window during diagenesis (Ortner & Sachsenhofer, 1996). Oil must have been produced from bituminous marls below the Tirolic nappe (S of Inn Valley in Fig. 1), overlying the Bajuvaric unit (N of Inn valley in Fig. 1), where Oligocene deposits have been drilled (Tollmann, 1986). The maximum possible temperature during precipitation of cement 1 is near 90°C, assuming a marine fluid. This temperature is in line with maximum temperatures in the basin according to the thermal model, but most probably the fluids were hydrothermal, and therefore hotter than the surrounding rock. Probably cement 1 was precipitated before the maximum temperature in the basin was reached.

Cements 1,2 and 3 are found in the same large calcite veins in Kalkbruch outcrop formed during Oligocene sinistral shearing along the Inntal fault (D2). Trace element analysis suggests increasing meteoric influence (see above). Temperatures calculated for cements 2 and 3 are constant or decreasing in relation to cement 1.

Other calcites related to Oligocene burial diagenesis (blocky spars and skalenohedral calcites) found along D2-faults in the basement of the basin show a wide range of isotopic and trace element compositions. Maximum temperatures (100-130°C) are recorded by calcites from the Glemm location, that show marine trace element composition. These calcites must have been precipitated from a hydrothermal fluid, because the basin never reached such high temperatures. Other cements rich in Mn record lower temperatures, possibly due to admixture of cold meteoric water to the diagenetic fluid.

Cements within the calcareous marls (saddle calcites) are chemically similar the the marls. Carbon isotope values of bulk samples of calcareous marls and saddle calcites are comparable. The diagenetic fluid in the calcareous marls was most probably generated by dewatering of the marls and is a marine fluid, and the oxygen isotopic values only relate to temperature. Early cementation related to soft sediment deformation took place at a temperature near 30°C, whereas saddle calcites found along sinistral NE-striking faults formed at a temperature of ca. 60°C. The overall chemical similarity between hostrock and cement suggests, that cementation within the calcareous marls took place in a closed system. The sinistral faults associated to the saddle calcites postdate D3-folding in the area, and rather are were active during D4.

References

Anderson, T. F. & Arthur, M. A. (1983): Stable isotopes of oxygen and carbon and their application to sedimentologic and paleoenvironmental problems. In: Arthur, M. A., Anderson, T. F., Kaplan, I. R., Veizer, J. & Land, L. S (Hrsg.): Stable isotopes in sedimentary geology, SEPM Short Course No. 10, 1/1–1/151, Dallas.

Craig, H. (1965): The measurement of oxygen isotope paleotemperatures. In: Tongiorgi, T. (Hrsg.): Stable isotopes in oceanographic studies and paleotemperatures, 1–24, Pisa (Consiglio Nazionale della Richerche, Laboratorio di Geologia Nucleare).

Czurda, A. & Bertha, S. (1984): Verbreitung und Rohstoffmäßige Eignung von Tonen und Tongesteinen in Nordtirol. Archiv für Lagerstättenforschung der Geologischen Bundesanstalt, 5, 15–28, 6 Abb., 5 Tab., Wien.

Erel, Y. & Katz, A. (1990): Trace-element distribution across calcite veins: a tool for genetic interpretation. Chemical Geology, 85, 361–367, 5 Abb., Amsterdam

Hubbert, M. K. & Rubey, W. W. (1959): Role of fluid pressure in mechanics of overthrust aulting, I, Mechanics of fluid-filled solids and its application to overthrust faulting. Geological Society of America Bulletin, 70, 115–166, Boulder.

Kinsman, D. (1969): Interpretation of Sr^{2+} concentrations in carbonate minerals and rocks. Journal of Sedimentary Petrology, 39, 486–508, 4 Abb., 9 Tab., Tulsa.

Krois, P. & Stingl, V. (1991): Faziesanalyse fluviatiler Sedimente – eine Fallstudie in den Oberangerberger

Schichten (Oberoligozän, Tirol). Jahrbuch der Geologischen Bundesanstalt, **134**, 299–308, 9 Abb., Wien.

Kuhlemann, J. (1995): Zur Diagenese des Karawanken-Nordstammes (Österreich/Slowenien) – spätriassische epigenetische Blei - Zink Vererzung und mitteltertiäre hydrothermale Karbonatzementation.- Archiv für Lagerstättenforschung der Geologischen Bundesanstalt, **18**, 57–116, 36 Abb., 25 Tab., 4 Taf., Wien.

Lohmann, K. C.(1988): Geochemical patterns of meteoric diagenetic systems and their application to studies of paleokarst. In: James, N. P. & Choquette, P. W. (Hrsg.): Paleokarst, 58–80, 13 Abb., New York (Springer).

Ortner, H.(1996): Deformation und Diagenese im Unterinntaler Tertiär (zwischen Rattenberg und Durchholzen) und seinem Rahmen. Unpubl. Diss. Univ. Innsbruck, 234 S., Innsbruck.

Ortner, H. (1999): Verformung von unverfestigten Sedimenten: Die Unterangerberger Schichten, Unterinntaler Tertiär, Tirol. Mitteilungen der Gesellschaft der Geologie und Bergbaustudenten Österreichs, **42**, 189–190, 3 Abb., Wien.

Ortner, H. & Sachsenhofer, R. (1996): Evolution of the Lower Inntal Tertiary and Constraints on the Development of the Source Area. In: Liebl, W. & Wessely, G. (Hrsg.): Oil and Gas in Alpidic Thrust Belts and Basins of Central and Eastern Europe, EAEG Spec. Publ. No. 5, 237–247, 8 Abb., 4 Tab., London.

Ortner, H. & Stingl, V. (2001): Facies and Basin Development of the Oligocene in the Lower Inn Valley, Tyrol/Bavaria. In: Piller, W. & Rasser, M. (Hrsg.): Paleogene in Austria, Schriftenreihe der Erdwissenschaftlichen Kommissionen, 14, 153–196, 24 Abb., Wien (Österreichische Akademie der Wissenschaften).

Peresson, H. & Decker, K. (1997): The Tertiary dynamics of the northern Eastern Alps (Austria): changing palaeostresses in a collisional plate boundary. Tectonophysics, **272**, 125–157, Amsterdam.

Petit, J. P. (1987): Criteria for the sense of movement on fault surfaces in brittle rocks. Journal of Structural Geology, **9/5–6**, 597–608, 10 Abb., Oxford.

Ratschbacher, L., Frisch, W., Linzer, G. & Merle, O. (1991): Lateral extrusion in the Eastern Alps, Part 2: Structural analysis. Tectonics, **10/2**, 257–271, 8 Abb., 1 Tab., Washington.

Scherbacher, M. (2000): Rekonstruktion der oligozänen Umweltentwicklung im Ostalpenraum anhand von Foraminiferen. Tübinger mikropaläontologische Mitteilungen, 23, 132 p., Tübingen.

Sibson, R. H. (1983): Continental Fault Structure and the Shallow Earthquake Source. Jour. Geol. Soc. London, **140**, 741–767, 11 Abb., 3 Tab., Belfast.

Sibson, R. H. (1994): Crustal stress, faulting and fluid flow. In: Parnell, J. (Hrsg.): Geofluids: Origin, migration and evolution of fluids in sedimentary basins, Geological Society of London Special Publication No. 78, 69–84, 9 Abb., 1 Tab., London.

Stingl, V. (1990): Die Häringer Schichten vom Nordrand des Unterinntaler Tertiär-Beckens (Angerberg/Tirol): Fazies, Sedimentpetrographie und beckengenetische Aspekte. Geol. Paläont. Mitt. Innsbruck, **17**, 31–38, Innsbruck.

Stingl, V. & Krois, P. (1991): Marine Fan Delta Development in a Paleogene Interior Alpine Basin (Tyrol, Austria). Neues Jahrbuch für Geologie und Paläontologie, Monatshefte, **7**, 427–442, Stuttgart.

Tollmann, A. (1986): Geologie von Österreich, Band 3. 718 p., 145 Abb., 8 Tab., 3 Taf., Wien (Deuticke).

Tucker, M. E. & Wright, V. P. (1990): Carbonate Sedimentology. 482 p., Oxford (Blackwell).

Weber, L. (1997): Handbuch der Lagerstätten der Erze, Industrieminerale und Energierohstoffe Österreichs. Archiv für Lagerstättenforschung der Geologischen Bundesanstalt, **19**, 607, Wien.

Zeeh, S., Kuhlemann, J. & Bechstädt, T (1995): Diagenetic Evolution of the Carnian Wettersteinkalk Platforms of the Eastern Alps. Sedimentology, **42**, 199–222, 16 Abb., 3 Tab., Oxford.

Zöbelein, H. K. (1955): Über Alttertiär - Gerölle aus der subalpinen Molasse des westlichen Oberbayerns und der inneralpinen Molasse (Angerbergschichten) des Tiroler Unterinntales (Vorläufige Mitteilung). Neues Jahrbuch für Geologie und Paläontologie, Monatshefte, **1955**, 343–348, Stuttgart.

Appendix

Tables of Isotope values, trace element concentrations and sampling locations.

Author's address:
Dr. Hugo Ortner, Institute of Geology and Paleontology, University of Innsbruck, Innrain 52, A-6020 Innsbruck
e-mail: Hugo.Ortner@uibk.ac.at

	Sample No.	δ^{13}C PDB	± Error	δ^{18}O PDB	± Error
0	A349	-1.2300	0.030000	-12.615	0.050000
1	BP1/1	0.22000	0.040000	-9.1904	0.080000
2	BP1/2	0.22000	0.020000	-8.5900	0.030000
3	BP2/1	1.6000	0.030000	-8.6666	0.050000
4	BP2/2	1.3100	0.030000	-8.4338	0.060000
5	BR2/1	-2.5100	0.030000	-2.4873	0.070000
6	BR2/2	-2.2000	0.050000	-4.8931	0.080000
7	BR2/4	-2.3300	0.020000	-4.5729	0.040000
8	DUX	-1.2100	0.030000	-9.3359	0.090000
9	EB	1.6100	0.070000	-2.5164	0.0100000
10	G1/2	-0.76000	0.040000	-4.3013	0.050000
11	G1/3	2.8300	0.020000	-5.1550	0.060000
12	G1/4	0.92000	0.020000	-10.859	0.050000
13	G1/5	-2.3900	0.090000	-13.012	0.090000
14	G3	-0.43000	0.030000	-1.5463	0.080000
15	G4/2/2	-9.2900	0.040000	-6.7265	0.060000
16	G4/2/3	-7.4500	0.040000	-6.6101	0.14000
17	G4/2/4	-11.060	0.040000	-6.9399	0.0100000
18	G4/2/5	-6.3700	0.10000	-5.3393	0.11000
19	G4/2/6	-7.5700	0.050000	-5.2908	0.090000
20	G4/2/7	-6.8000	0.12000	-5.4945	0.20000
21	G4/2/8	-7.7400	0.070000	-5.8631	0.080000
22	G4/2/9	-3.0300	0.020000	-4.8445	0.020000
23	G4/5/1	-7.5300	0.050000	-5.7661	0.040000
24	G4/5/2	-7.0300	0.080000	-5.4945	0.030000
25	G4/5/3	-7.2500	0.090000	-5.4751	0.12000
26	G4/5/4	-7.3800	0.050000	-5.6109	0.060000
27	G4/5/5	-8.3200	0.13000	-6.5519	0.11000
28	G8/2	4.0500	0.030000	-4.0879	0.090000
29	G8/4	4.2500	0.030000	-6.1929	0.090000
30	G8/6	4.0500	0.12000	-3.6029	0.080000
31	G9	3.9800	0.040000	-7.5316	0.080000
32	GB2	-0.99000	0.080000	-9.4620	0.060000
33	GB3	-6.2700	0.030000	-4.8542	0.030000
34	GL1/1	-0.52000	0.040000	-17.252	0.060000
35	GL1/2	-4.9300	0.0100000	-14.303	0.040000
36	KB1/1	-2.5800	0.030000	-14.468	0.050000
37	KB1/2	-3.7400	0.030000	-14.371	0.050000
38	KB1/3	-2.5300	0.0100000	-16.679	0.020000
39	KB1/4	-1.8300	0.020000	-17.106	0.050000
40	KB2/1	-0.94000	0.030000	-3.6126	0.060000
41	KB2/2	-11.520	0.030000	-3.2439	0.050000
42	KB2/3	-4.9700	0.030000	-14.545	0.080000
43	KB2/5	-4.8700	0.060000	-14.691	0.10000
44	KB2/6	-3.7800	0.15000	-6.2996	0.13000
45	KB3/1	4.1700	0.040000	-2.7686	0.050000
46	KB3/2	3.5200	0.040000	-3.7581	0.060000
47	KB4/2	3.2300	0.030000	-4.0200	0.040000
48	KB4/3	-5.1000	0.020000	-12.799	0.050000
49	KB4/5	-4.6800	0.020000	-12.925	0.040000
50	KB4/6	-1.2500	0.040000	-7.0078	0.080000
51	KB4/7	-1.9700	0.020000	-7.1436	0.050000
52	KB5/1	2.8300	0.030000	-4.5729	0.030000
53	KB5/3	-5.4200	0.030000	-13.362	0.050000
54	KB5/4	-2.6800	0.020000	-16.252	0.060000
55	KB5/5	-2.3300	0.030000	-16.175	0.030000
56	KB8/1	-0.64000	0.060000	-11.004	0.050000
57	KB8/2	0.32000	0.040000	-15.069	0.040000
58	MB14	2.4900	0.040000	-2.0799	0.050000
59	MB26	1.9900	0.060000	-1.4687	0.080000
60	MB3/1	0.10000	0.030000	-3.7484	0.070000
61	MB9	2.1600	0.070000	-1.2941	0.070000
62	OF10a/1	-2.4800	0.030000	-17.853	0.050000
63	OF10a/2	-2.4600	0.050000	-17.999	0.070000
64	OF10b/2	-1.4700	0.020000	-17.242	0.060000
65	OF1b/1	0.80000	0.070000	-1.8859	0.090000
66	OF1b/2	0.48000	0.050000	-3.5447	0.060000
67	OF2/1	0.87000	0.020000	-2.9917	0.020000
68	OF2/2	0.85000	0.020000	-3.0596	0.070000
69	OF2/3	1.0100	0.050000	-0.57628	0.070000
70	OF2/4	1.0600	0.050000	-0.45018	0.090000
71	OF2/5	1.0400	0.070000	-0.71209	0.080000
72	PE	1.8600	0.030000	-3.4671	0.030000
73	UAS1	0.86000	0.030000	-3.0887	0.030000
74	UAS2	0.060000	0.0100000	-3.0984	0.060000

Table 1: C– and O-isotope values of the samples measured. For exact location and characterisation of samples, see Table 3.

	Probe	Mg ppm	Fe ppm	Mn ppm	Ba ppm	Sr ppm	Zn ppm
0	A349	3181.2	3700.8	359.55	19.663	511.24	1.4045
1	BP1/1	2032.1	3612.2	118.59	0.0000	1341.3	3.2051
2	BP1/2	2079.4	4007.8	129.41	0.0000	1176.5	0.0000
3	BR2/1	2663.9	933.33	133.33	16.667	338.89	16.667
4	BR2/2	2777.8	682.10	114.20	33.951	330.25	18.519
5	BR2/4	2219.9	951.39	138.89	16.204	365.74	11.574
6	BR2/4*	2004.6	812.50	141.20	11.574	472.22	6.9444
7	DUX1	5567.5	88.710	752.02	22.177	68.548	0.0000
8	EB	1111.4	1041.2	410.36	16.704	285.63	1.1136
9	G1/2	5508.2	38.174	14.222	2.2455	190.87	3.7425
10	G1/3	9744.7	47.368	7.8947	0.0000	250.00	7.8947
11	G1/4	2861.3	254.57	13.720	0.0000	443.60	4.5732
12	G1/5	1023.5	176.98	23.515	1.2376	586.63	2.4752
13	G3	4858.0	1445.3	269.33	14.667	350.00	41.333
14	G4/2/2	2302.5	282.50	105.00	22.500	217.50	7.5000
15	G4/2/3	1078.9	72.368	52.632	13.158	92.105	6.5789
16	G4/2/4	1660.3	119.66	106.84	21.368	170.94	6.4103
17	G4/2/5	617.05	8.6705	13.006	2.8902	53.468	1.4451
18	G4/2/6	1028.2	241.20	123.24	19.366	156.69	12.324
19	G4/2/7	483.33	133.33	16.667	0.0000	50.000	33.333
20	G4/2/8	2241.9	354.84	69.892	32.258	147.85	10.753
21	G4/5/1	2199.6	441.53	90.726	22.177	125.00	12.097
22	G4/5/2	1011.2	294.78	52.239	7.4627	63.433	26.119
23	G4/5/3	1002.0	242.13	110.24	13.780	139.76	11.811
24	G4/5/4	793.48	14.493	10.870	3.6232	50.725	7.2464
25	G4/5/5	2046.3	151.23	83.333	24.691	194.44	10.802
26	G8/2&5	2214.6	3.9370	0.10000	0.0000	165.35	3.9370
27	G8/4	1265.7	1.5723	0.10000	0.0000	227.99	0.0000
28	G8/6	2420.2	2.6596	0.10000	0.0000	216.76	2.6596
29	G9	1117.6	2.2624	2.2624	0.0000	79.186	1.1312
30	GB2	1368.5	3312.0	253.70	13.889	359.26	16.667
31	GB3	219.41	29.720	0.87413	0.87413	19.231	6.9930
32	GL1/1	1707.7	5.2910	27.778	0.0000	349.21	0.0000
33	GL1/2	17677	99.558	32.080	0.0000	241.15	1.1062
34	KB1/1	1765.2	6.5217	167.39	23.913	236.96	0.0000
35	KB1/2	1414.3	4.2857	125.71	15.714	142.86	1.4286
36	KB1/3	1432.4	27.027	60.811	81.081	155.41	0.0000
37	KB1/4	1664.5	32.895	111.84	65.789	125.00	0.0000
38	KB2/1	2900.7	10.274	0.10000	34.247	147.26	20.548
39	KB2/2	1150.5	60.185	13.889	18.519	46.296	6.9444
40	KB2/3	2754.1	8.1301	107.72	111.79	302.85	6.0976
41	KB2/4	1495.0	5.0336	62.081	0.0000	85.570	0.0000
42	KB2/6	1879.6	854.94	67.901	3.0864	92.593	15.432
43	KB3/1	2807.0	2.5907	10.363	2.5907	182.64	3.8860
44	KB3/2	4756.6	141.45	108.55	16.447	171.05	29.605
45	KB4/2	2768.0	4.9020	22.876	1.6340	196.08	3.2680
46	KB4/3	2601.4	3.3784	96.284	1.6892	410.47	5.0676
47	KB4/5	2500.0	2.7624	80.110	2.7624	473.76	1.3812
48	KB4/7	1388.0	4.6012	61.350	4.6012	306.75	1.5337
49	KB5/1	2271.7	156.67	6.6667	0.0000	166.67	3.3333
50	KB5/2	2573.9	8.5227	42.614	0.0000	406.25	5.6818
51	KB5/4	1406.0	4.2735	32.051	0.0000	145.30	8.5470
52	KB8	1195.7	2.2624	38.462	1.1312	122.17	3.3937
53	MB14	9962.1	5256.6	87.121	18.939	2694.1	29.356
54	MB26	11563	9019.0	1159.5	170.25	1034.8	39.241
55	MB9	10533	7738.2	305.79	27.897	1892.7	35.408
56	OF10a	2917.0	973.74	143.91	220.06	231.09	1.5756
57	OF10b	2041.2	1029.2	153.78	590.21	234.54	0.0000
58	OF1b/1	2252.2	216.59	7.5431	4.3103	248.92	4.3103
59	OF1b/2	1951.0	4.9834	0.10000	4.1528	191.86	2.4917
60	OF2/1	3651.4	42.254	3.5211	7.0423	482.39	3.5211
61	OF2/2	3777.5	2.7473	0.10000	13.736	505.49	2.7473
62	PE	1866.8	2956.2	233.58	27.372	2104.0	5.4745

Table 2: Trace element concentration of the samples measured.

	sample No.	Y_M BMN	X_{GKM} BMN	sample description
0	A349	362450	266375	blocky spar
1	BP1/1	359000	262775	bulk sample of calcareous marls
2	BP1/2	359000	262775	bulk sample of calcareous marls
3	BP2/1	359000	262775	saddle calcite
4	BP2/2	359000	262775	saddle calcite
5	BR2/1	356125	262500	Oligocene carbonate, non-luminescent
6	BR2/2	356125	262500	Oligocene carbonate, luminescent
7	BR2/4	356125	262500	Oligocene carbonate, non-luminescent
8	DUX	363650	272525	blocky spar
9	EB	362570	268037	skalenohedral calcite
10	G1/2	355950	262525	Wetterstein limestone, "Großoolith"
11	G1/3	355950	262525	Wetterstein limestone, "Großoolith"
12	G1/4	355950	262525	skalenohedral calcit
13	G1/5	355950	262525	skalenohedral calcit
14	G3	355950	262525	calcareous marls in fissure
15	G4/2/2	355950	262525	tufa crust
16	G4/2/3	355950	262525	speleothem
17	G4/2/4	355950	262525	tufa crust
18	G4/2/5	355950	262525	speleothem
19	G4/2/6	355950	262525	tufa crust
20	G4/2/7	355950	262525	skalenohedral calcit
21	G4/2/8	355950	262525	tufa crust,"terrestrial stromatolite"
22	G4/2/9	355950	262525	skalenohedral calcit
23	G4/5/1	355950	262525	tufa crust,"terrestrial stromatolite"
24	G4/5/2	355950	262525	skalenohedral calcit
25	G4/5/3	355950	262525	tufa crust
26	G4/5/4	355950	262525	speleothem
27	G4/5/5	355950	262525	tufa crust
28	G8/2	355950	262525	radial-fibrous calcite in Wetterstein limestone
29	G8/4	355950	262525	blocky spar in Wetterstein limestone
30	G8/6	355950	262525	bulk sample, Wetterstein limestone
31	G9	355950	262525	blocky spar in Wetterstein limestone
32	GB2	355950	262525	calcareous marls in fissure
33	GB3	355950	262525	speleothem
34	GL1/1	361750	270200	skalenohedral calcit
35	GL1/2	361750	270200	skalenohedral calcit
36	KB1/1	359400	264000	cement 2
37	KB1/2	359400	264000	cement 2
38	KB1/3	359400	264000	cement 3
39	KB1/4	359400	264000	cement 3
40	KB2/1	359400	264000	bulk sample, Wetterstein limestone
41	KB2/2	359400	264000	speleothem
42	KB2/3	359400	264000	cement 1
43	KB2/5	359400	264000	cement 1
44	KB2/6	359400	264000	tufa crust
45	KB3/1	359400	264000	We, bulk sample
46	KB3/2	359400	264000	radial-fibrous calcite in Wetterstein limestone
47	KB4/2	359400	264000	bulk sample, Wetterstein limestone
48	KB4/3	359400	264000	cement 1
49	KB4/5	359400	264000	cement 1
50	KB4/6	359400	264000	cement 2
51	KB4/7	359400	264000	cement 2
52	KB5/1	359400	264000	bulk sample, Wetterstein limestone
53	KB5/3	359400	264000	cement 1
54	KB5/4	359400	264000	cement 2
55	KB5/5	359400	264000	cement 2
56	KB8/1	359400	264000	Kanonenspat
57	KB8/2	359400	264000	Kanonenspat
58	MB14	359000	262775	bulk sample, calcareous marls
59	MB26	359000	262775	bulk sample, calcareous marls
60	MB3/1	359000	262775	Oligocene carbonate, bulk sample, luminescent
61	MB9	359000	262775	bulk sample, calcareous marls
62	OF10a/1	358889	264678	cement 3
63	OF10a/2	358889	264678	cement 3
64	OF10b/2	358889	264678	cement 3
65	OF1b/1	358889	264678	Oligocene carbonate, bulk sample, non-luminescent
66	OF1b/2	358889	264678	Oligocene carbonate, bulk sample, non-luminescent
67	OF2/1	358889	264678	Oligocene carbonate, bulk sample, non-luminescent
68	OF2/2	358889	264678	Oligocene carbonate, bulk sample, non-luminescent
69	OF2/3	358889	264678	Nummulit
70	OF2/4	358889	264678	Nummulit
71	OF2/5	358889	264678	Nummulit
72	PE	359400	264000	Oligocene carbonate, bulk sample, non-luminescent
73	UAS1	352369	261717	saddle calcite
74	UAS2	352369	261717	saddle calcite

Table 3: Geographical coordinates of sampling localities and short description of sample. n. = non-luminescent, l. = luminescent